

Cocrystal Structures of NC6.8 Fab Identify Key Interactions for High Potency Sweetener Recognition: Implications for the Design of Synthetic Sweeteners[†]

Kuppan Gokulan,[‡] Sangeeta Khare,[§] Donald R. Ronning,^{‡,||} Scott D. Linthicum,^{‡,§} James C. Sacchettini,^{*,‡} and Bernhard Rupp^{*,‡,⊥}

Department of Biochemistry & Biophysics, Texas A&M University, College Station, Texas 77843-2128, Department of Veterinary Pathobiology, Texas A&M University, College Station, Texas 77843-4467, and Lawrence Livermore National Laboratory, University of California, Livermore, California 94551

Received April 2, 2005; Revised Manuscript Received May 25, 2005

ABSTRACT: The crystal structures of the murine monoclonal IgG2b(κ) antibody NC6.8 Fab fragment complexed with high-potency sweetener compound SC45647 and nontasting high-affinity antagonist TES have been determined. The crystal structures show how sweetener potency is fine-tuned by multiple interactions between specific receptor residues and the functionally different groups of the sweeteners. Comparative analysis with the structure of NC6.8 complexed with the super-potency sweetener NC174 reveals that although the same residues in the antigen binding pocket of NC6.8 interact with the zwitterionic, trisubstituted guanidinium sweeteners as well as TES, specific differences exist and provide guidance for the design of new artificial sweeteners. In case of the nonsweetener TES, the interactions with the receptor are indirectly mediated through a hydrogen bonded water network, while the sweeteners bind with high affinity directly to the receptor. The presence of a hydrophobic group interacting with multiple receptor residues as a major determinant for sweet taste has been confirmed. The nature of the hydrophobic group is likely a discriminator for super- versus high-potency sweeteners, which can be exploited in the design of new, highly potent sweetener compounds. Overall similarities and partial conservation of interactions indicate that the NC6.8 Fab surrogate is representing crucial features of the T1R2 taste receptor VFTM binding site.

Taste Perception. The sensation of taste plays a critical role in the life and nutritional habits of humans and other organisms (1). The perception of taste is elicited through the interaction of tastants with their receptors in the taste cells (2). It is widely believed that humans perceive five qualities of taste: the four basic perceptions sour, salty, bitter, and sweet (2–4) and umami, the taste of substances related to L-glutamate (5). The chemical nature of tastants varies widely and includes ions, small organic molecules, proteins, carbohydrates, and amino acids. Sweet and umami tastants mediate perception by interacting with distinct subclass 3 (C) G-protein-coupled T1R surface receptors that are expressed in a subset of epithelial taste cells. A characteristic of the class 3 GPCRs¹ is the presence of a distinct, two-lobed, extracellular Venus fly trap module (VFTM), and the formation of either homo- or heterodimers (6).

During the past years, significant progress has been made in identification (7), functional expression, and characterization of taste receptors from mammals (5, 8, 9). Sweet taste perception generally requires a heterodimer of the T1R2 and T1R3 receptor, with the cysteine rich linker region between the extracellular VFTM and the seven-helix transmembrane spanning region of the T1R3 receptor identified as an additional key factor in the recognition of peptide/protein sweeteners (10). Structures of several sweet-tasting proteins have been determined by NMR (11, 12), but the functional groups which are responsible for taste perception have still to be determined, largely due to the lack of sequence and structural homology (13) among the sweet-tasting peptides.

Recent investigations of the heteromeric T1R receptor family confirm different functional roles of the subunits as well as the presence of discrete sites responsible for binding chemically different ligands (14), demonstrating that a single orthosteric binding site assumed in the classical pharmacophore models (15) does not universally cover all types of sweet tastants (16).

Modeling studies based on the crystal structure of bovine rhodopsin (17) combined with experimental mutational screening indicate that also residues within the transmem-

[†] This study was supported by NIH P50 Grant GM62410 and by the Robert Welch Foundation at Texas A&M University.

* Authors to whom correspondence should be addressed. B.R.: LLNL-BBRP, L448, University of California, Livermore, CA 94551; e-mail, br@llnl.gov; tel, 925-423-3273. J.C.S.: Department of Biochemistry & Biophysics, Texas A & M University, College Station, TX 77843-2128; e-mail, Sacchett@tamu.edu; tel, 979-862-7636.

[‡] Department of Biochemistry & Biophysics, Texas A&M University.

[§] Department of Veterinary Pathobiology, Texas A&M University.

^{||} Current address: Laboratory of Molecular Biology, National Institute of Diabetes and Digestive and Kidney Diseases, Bethesda, MD.

[⊥] Lawrence Livermore National Laboratory, University of California.

¹ Abbreviations: mAB, monoclonal antibody; Fab, antibody fragment; CDR, complementarity determining region; TES, *N*-[tris(hydroxymethyl)methyl]-2-aminoethanesulfonic acid; GPCR, G-protein coupled receptor; VFTM, Venus fly trap module; PEG, poly ethylene glycol.

brane region of hT1R3 play a key role in the binding of lactisole, a broad acting sweet taste antagonist (18), further attesting to the complexity of the mechanism of taste perception. The determination of the metabolic glutamate receptor mGluR1 ligand binding region (19) and the availability of T1R sequences (20) would in principle allow modeling of sweet tastant binding sites expected to be located at the interface between the two lobes of the extracellular T1R2 VFTM modules. However, the significant interdomain movement and conformational changes involved in the clamshell type binding mechanism, combined with the relocation of dimer interfaces (19), are rather challenging to model with the accuracy necessary for reliable docking studies.

In view of the difficulty to obtain crystal structures of intact G-protein-coupled cell surface receptors, we have pursued an alternative approach based on the comparative analysis of crystal structures of synthetic substituted triguanidine sweetener and nonsweetener compounds complexed with murine monoclonal antibody (mAB) NC6.8.

Antibody Complex Crystal Structures as Glucophore Binding Models. Several different models have been developed to describe the nature and topological arrangement of glucophores in an ideal sweet compound. A model for a receptor site with electrostatic potential, hydrogen bonding potential, and hydrophobic interactions has been proposed to match the properties of low-energy conformers of various sweeteners (21). The crystal structure of super-potency sweetener compound NC174, a zwitterionic, trisubstituted guanidine hapten, complexed with NC6.8 IgG2b(κ) mAB raised against NC174, has been reported (22). Interestingly, NC14.10, an isotype IgG2b(λ) mAB, displayed a significantly different binding mode against the same hapten, attesting to the structural diversity in antigen recognition by immunoglobulins (23). A comprehensive summary of the monoclonal antibody libraries that recognize super sweeteners has been published (24).

To further investigate the structural basis for the recognition of substituted triguanidine tastants, we analyzed the cocrystal structures of the NC6.8 Fab fragment, serving as a structural surrogate for the elusive taste receptor complex. NC6.8 was cocrystallized with SC45647 (25), a high-potency sweetener structurally close to super sweetener NC174 (Figure 1), and with non-sweet-tasting TES (*N*-[tris(hydroxymethyl)methyl]-2-aminoethanesulfonic acid). The analysis of super-potency (NC174, 200 000 times sweeter than 2% sucrose) and high-potency sweeteners (SC45647, 28 000 times sweeter) versus a nonsweetening compound allows the identification of key molecular interactions specifying the structure–activity relationship of zwitterionic sweet-tasting molecules (Figure 1). The complex crystal structures show that both sweetener compounds as well as TES bind in the antigen binding pocket, but exhibit significant differences in binding patterns as well as in placement of the hydrophobic moieties, and reveal the role of specific interactions in the recognition and design of super-potency versus high-potency sweetener compounds.

MATERIALS AND METHODS

Purification of Antibodies. Murine NC6.8 IgG2b(κ) antibodies were first precipitated from ascites fluid with 60% saturated ammonium sulfate precipitation as described (26).

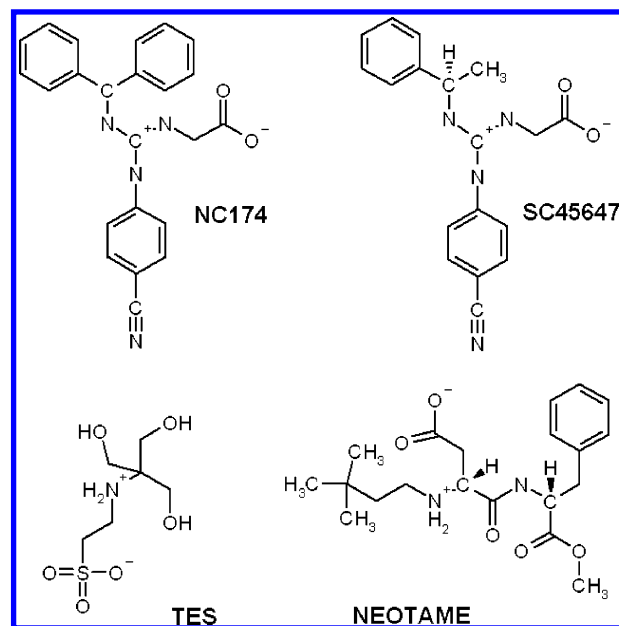


FIGURE 1: Zwitterionic sweet-tasting molecules and TES. NC174 represents a trisubstituted guanidinium super-potency sweetener (200 000 times sweeter than 2% sucrose), SC45647 is a high-potency tastant (28 000 times sweeter) of the same family, neotame represents a medium-potency dipeptide derived sweetener, and zwitterionic TES is not sweet tasting.

The precipitate was collected after centrifugation for 10 min at 10,000g, then resuspended (2 mg/mL concentration), and dialyzed against 20 mM phosphate buffer (pH 7.2) overnight. The dialyzed sample was loaded onto an IgG column and washed thoroughly with phosphate. The bound antibodies were eluted with 0.1 M glycine-HCl buffer (pH 2.8), and the eluent was immediately neutralized with 1 M Tris pH 9.0. The affinity purified IgG was concentrated (6 mg/mL) using a Centrprep concentrator and digested by papain.

Papain (type III, 2 × crystallized from Sigma) was initially activated with cysteine as described (27). Proteolysis was carried out at 37 °C in 0.1 mM sodium acetate buffer pH 5.5 containing 3 mM EDTA and 50 mM cysteine. After 4 h proteolysis was stopped by addition of iodoacetamide (to alkylate the sulfhydryl groups) at a final concentration of 30 mM and the reaction products were centrifuged for 30 min at 10,000g. The supernatant was loaded onto a 2.5 × 100 cm high-resolution Sephacryl S-200 (Pharmacia) column equilibrated at pH 8.0 with 25 mM Tris-HCl, 0.1 M NaCl, 1 mM Na₃N. The Fab eluted as the last peak, well separated from Fc fragments and uncleaved antibodies. Prior to crystallization trials, the purified antibody fragment solutions were concentrated to 40 mg/mL and dialyzed against 20 mM TES buffer, pH 6.8 and diluted to a final concentration of 15 mg/mL.

Crystallization. NC6.8 Fab (10–15 mg/mL) was incubated (1 h) with compound SC45647 at a 2-fold molar excess. Initial crystallization conditions were screened in hanging drops (28) using a sparse matrix kit (Crystal Screen I, Hampton Research, CA). Small crystals of the NC6.8–SC45647 complex grew in 2 days at 18 °C from 4 μ L sitting droplets consisting of a 1:1 mixture of stock NC6.8–SC45647 complex and a crystallization buffer containing 50 mM potassium hydrogen phosphate pH 9.2 containing 20% PEG 8000. Crystallization conditions were refined until crystals about 0.2 mm in size could be obtained in a

Table 1: Data Collection and Refinement Statistics for NC6.8–SC45647 and NC6.8–TES Complexes

data collection	NC6.8–SC45647	NC6.8–TES
PDB ID code	1YNK	1YNL
space group	C2	C2
wavelength (Å)	1.0000	1.0000
temperature (K)	120	120
<i>a</i> (Å)	135.6	136.2
<i>b</i> (Å)	48.19	48.14
<i>c</i> (Å)	75.35	76.09
β (deg)	109.04	109.50
resolution (Å)	23.64–2.1	23.25–1.7
highest resolution bin (Å)	2.2–2.1	1.75–1.7
observed reflections ^a	813664 (58014)	276375 (19682)
unique reflections ^a	24844 (2309)	43252 (2444)
% completeness ^a	92.7 (71.1)	85.0 (69.0)
<i>R</i> (merge) ^a	0.07 (0.32)	0.03 (0.10) ^g
$\langle I/\sigma \rangle$ ^a	8.8 (2.9)	26.9 (9.3) ^g
<i>V</i> _m (Matthews coefficient)	2.43	2.46
% solvent	49.4	49.9
refinement		
free <i>R</i> value, random, 5% ^a	0.277 (0.367)	0.241 (0.350)
<i>R</i> value	0.216 (0.272)	0.208 (0.232)
protein residues	438	438
water molecules	126	247
SC45647	1	0
TES	0	1
rmsd bond length (Å) ^b	0.027	0.015
rmsd bond angle (Å) ^b	2.459	1.828
overall coordinate error (Å) ^c	0.23	0.13
RSCC (Shake&wARP) ^d	0.93	0.94
RSCC (Refmac5) ^e	0.95	0.95
Ramachandran appearance ^f		
most favored (number, %)	329 (88.4)	337(90.6)
allowed (number, %)	37(9.9)	29(7.8)
generously allowed (number, %)	3 (0.8)	4 (1.1)
disallowed (number, %)	3 (0.8)	2 (0.5)

^a Values in parentheses for the highest resolution bin. ^b Deviations from restraint targets (43). ^c Estimated standard uncertainty, diffraction precision index (DPI) based on *R* free (44). ^d Real space correlation coefficient, *F*_c map against averaged and weighted Shake&wARP map (34). ^e Real space correlation coefficient, *F*_o map against *F*_c map, as reported by Refmac5 (35). ^f Regions as defined in PROCHECK (42). ^g Due to detector positioning limitations, data could not be collected with sufficient completeness to full resolution limit.

reproducible manner within 3–4 days. Low-potency sweetener compounds NC90, NC24, NC274, and aspartame were incubated in 100-fold molar excess with the NC6.8 Fab fragment. Crystals grew under identical conditions and appeared within one to two weeks.

Data Collection. Crystals were harvested in Hampton cryoloops and flash-cooled directly in the nitrogen cold stream (120 K) after brief soaks in 2 μ L of mother liquor plus 2 μ L of 20% ethylene glycol as a cryoprotectant. Diffraction data were collected to 2.1 Å from a single crystal of NC6.8–SC45647 and to 1.7 Å data for NC6.8–TES at beam line 19 at the Advanced Photo Source of the Argonne National Laboratory with a 4 \times 4 module CCD detector. The data were reduced using DENZO (29), and intensities were scaled in space group C2 with SCALEPACK (29). Solvent content estimates (30, 31) indicated the presence of one monomer in the asymmetric unit. Data collection statistics are summarized in Table 1.

Structure Determination of NC6.8–SC45647 and NC6.8–TES. Initial phases for the NC6.8–SC45647 complex and the TES-bound crystal form were obtained by molecular replacement using the program CNS (32). The native NC6.8 Fab structure (1CGR) was used as a search model (22).

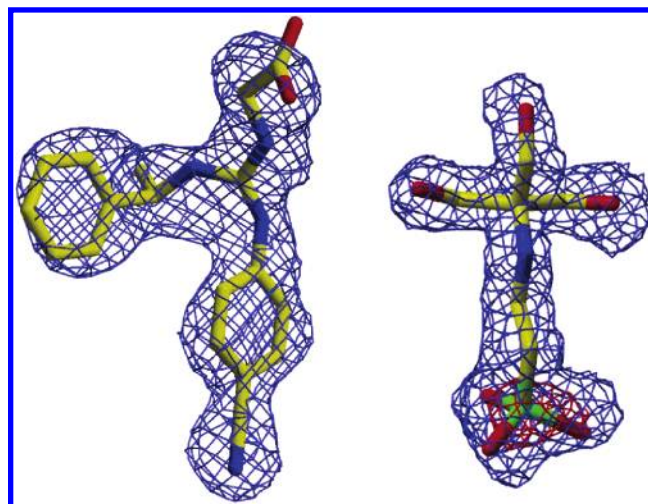


FIGURE 2: Electron density of ligands complexed with NC6.8 antibody. Electron density of SNW omit maps contoured at 1 σ level (blue grid) and 5 σ (red). Left panel: SC45647. Right panel: TES. In both cases the ligands are oriented corresponding to Figure 4a–c, pointing down into the antigenic binding pocket. Ligand molecules were omitted from the model before the SNW map generation. The blob feature in XtalView has been used to limit the display of the electron density to within 1.9 Å of the model. Figures created by XtalView (33) and rendered with Raster3d (46).

Separate cross-rotation functions for the variable and constant regions gave reliable solutions (data between 25 and 3.5 Å). The best solutions from the rotation search were used in the subsequent translation search carried out on a 0.25 Å grid, yielding strong and well-packing solutions.

The initial molecular replacement models were manually rebuilt with the program Xfit (33) into bias minimized, multiple averaged electron density maps obtained from the SNW (Shake&wARP) server (34), and refined with REFMAC5 (35). After repeated cycles of refinement and manual building, water molecules were manually added to the model using the SNW map, and clear electron density allowed unambiguous placement of the high-affinity ligand SC45647 in the SNW maps (Figure 2). The low-affinity ligand–Fab complex crystals revealed no density that was compatible with the incubated ligands. Instead, the binding sites contained a TES buffer molecule, which could be built unambiguously into the maps (Figure 2).

The completed models including SC45647 or TES, respectively, were submitted to a final round of refinement with REFMAC5 (Table 1). The final SNW electron density maps were of high quality, and density for residues L1–L214 of the L-chain (total of 219 residues) and H1–H158 and H164–H215 of the H-chain (also 219 residues) was clear; residues H159–H163 were less well defined. The antibody fragment residues were numbered following the numbering scheme for immunoglobulin by Kabat (36).

RESULTS

Overall Structure of the Complex Structures

The sweeteners NC174 and SC45647 and non-sweet-tasting TES buffer all bind in the same antigen-binding pocket of the NC6.8 antibody fragment (Figure 3). The binding pocket is formed by residues from CDR loops H1, H2, H3, L1, and L3 of the Fab fragment. The overall

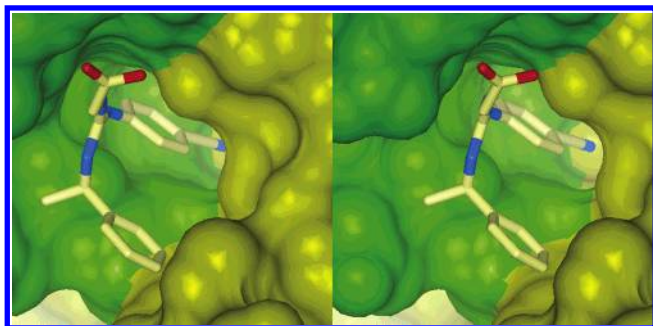


FIGURE 3: Cross-eyed stereoview of SC45647 in the NC6.8 antigen-binding pocket. Surface representation of the Fab molecule (light-chain residues, yellow; heavy-chain residues, green) emphasizing the deep antigen-binding pocket (view down into the pocket) of the NC6.8 occupied by high-potency sweetener SC45647. Ligand molecules are represented as ball-and-stick models, rendered with ICM Pro (41).

structure of NC6.8 is typical for IgG2b(κ) antibody Fab fragments, and has been described previously (22).

Binding of High-Potency Sweetener SC45647

The antigen-binding pocket of NC6.8 is highly complementary to high-potency sweetener SC45647, burying 565 Å² of the molecular surface. The ligand is clearly identifiable as the (*R*) stereoisomer with its chiral center at C8 (Figure 2). Most of the ligand atoms participate in hydrophobic interactions with residues from both the heavy chain and the light chain of NC6.8, with distinct hydrogen bonds to Glu 50H, Ser 97H, and Arg 56H (Figure 4a). The CN group of SC45647, in the same position as in the NC174 complex (Figure 5), is sandwiched between Gly 91L and Tyr 96L and hydrogen bonded to Ser 97H. It interacts indirectly via a conserved water molecule with two light-chain residues Ser 89L and Tyr 36L, an interaction pattern also observed in the NC174 complex. The cyanophenyl ring of SC45647 participates in π -stacking with aromatic tyrosine Tyr 96L, with a ring-to-ring distance of ~ 3.5 Å typical for π -stacking. The unsubstituted phenyl ring of SC45647 is accommodated at the entrance of the antigen-binding pocket and interacts through hydrophobic contacts primarily with Tyr 32L. The adjacent SC45647 methyl group exhibits weak hydrophobic interactions with the π -system of Tyr 96H. The trisubstituted guanidyl group of SC45647 π -stacks nicely with Trp 33H on one side, and has weak hydrogen bonds to the carboxyl group of Glu 50H and to Tyr 96H O η . On the other side, the guanidyl group forms weak hydrogen bonded contacts to Glu 50H and Tyr 96H. The SC45647 acetyl group is hydrogen bonded to N δ 2 of Asn 58H and N ϵ of the guanidyl group of Arg 56H, again in a conformation and interaction pattern similar to NC174 (Figure 4c). Electron density indicates the possibility of a minor conformation of the SC45647 acyl group, consistent with an alternate conformation of Arg 56H.

Binding of TES Buffer

When cocrystallization of low-affinity sweetener compounds NC90 (200 times sweeter than sucrose), NC24 (230 \times), NC274 (130 \times), and aspartame (150 \times) in 100-fold molar excess with NC6.8 Fab antibodies was attempted, none of the low-affinity sweetener compounds could be detected in the antigen-binding pocket. Clear electron density, how-

ever, was visible for TES protein stock buffer in the antigen-binding pocket (Figure 2) instead of the expected low-affinity sweetener compounds in all cocrystal structures. Zwitterionic TES (*N*-[tris(hydroxymethyl)methyl]-2-aminoethanesulfonic acid) essentially consists of an electronegative sulfonyl group with a short, two-carbon linker to a positively charged tris(hydroxymethyl)methyl-amino group.

The electronegative sulfonyl group of TES, located deep in the antigen-binding pocket, forms an extensive network of hydrogen bonds with residues of the antigen-binding pocket. In particular, the main chain amide hydrogens of Tyr 96H and Ser 98H, together with side chain interactions to His 34L and to Ser 89L via a tightly bound water atom, constitute a cluster of hydrogen bonded interactions that coordinate all three oxygen atoms of the sulfonyl group (Figure 4b). The tris(hydroxymethyl)methyl-amino group of TES is exposed to solvent, and its positively charged N1 interacts via a water molecule with Ser 98H. The three hydroxymethyl groups interact through a water mediated hydrogen bond network with both backbone and side chain atoms of numerous residues (Figure 4b). The positions of the respective carboxyl groups in both sweetener structures versus the sulfonyl group of TES do not coincide. Instead, the TES sulfonyl group occupies the approximate position of the CN group in the sweeteners (Figure 5), deep in the antigen-binding pocket of NC6.8. In agreement with the chemistry of the zwitterionic ligand, there are only few hydrophobic interactions compared to the NC174 and SC45647 molecules.

In an attempt to still obtain low-potency sweetener–Fab complexes, NC6.8 Fab was dialyzed against phosphate or Tris buffers instead of TES buffer. Unfortunately, attempts to crystallize NC6.8 in non-TES buffers with or without sweetener compounds have failed so far. We speculate that the TES may play an unexplained but critical role in the crystallization of the NC6.8 Fab under the conditions investigated.

DISCUSSION

Structural Comparison of the NC6.8–SC45647 and NC6.8–NC174 Sweetener Complexes

General. The sweetener ligands NC174 and SC45647, as well as TES buffer, bind in the same antigenic pocket, formed by residues from CDR loops H1, H2, H3, L1, and L3 of the NC6.8 Fab fragment (Figure 4a–c). NC174 and SC45647 are trisubstituted guanidine tastants. Both synthetic sweeteners contain a distinct electronegative cyanophenyl group, a zwitterionic guanidyl core, an acetyl group, and a large hydrophobic group. Substitution of one phenyl group in NC174 with a methyl group in SC45647 creates a chiral center at C8, and causes a reduction of super-sweetener potency by nearly 1 order of magnitude. Although the NC6.8 monoclonal antibody was raised against the NC174 sweetener, it recognizes both NC174 and the *R*-stereoisomer of SC45647 in a similar fashion.

In both binary complexes, the cyanophenyl group occupies the same position (Figure 5) and is deeply buried in the antigen-binding pocket. As described in detail for SC45647, in both cases the cyanophenyl group is sandwiched between the light chain and heavy chain by π -stacking to Tyr 96L

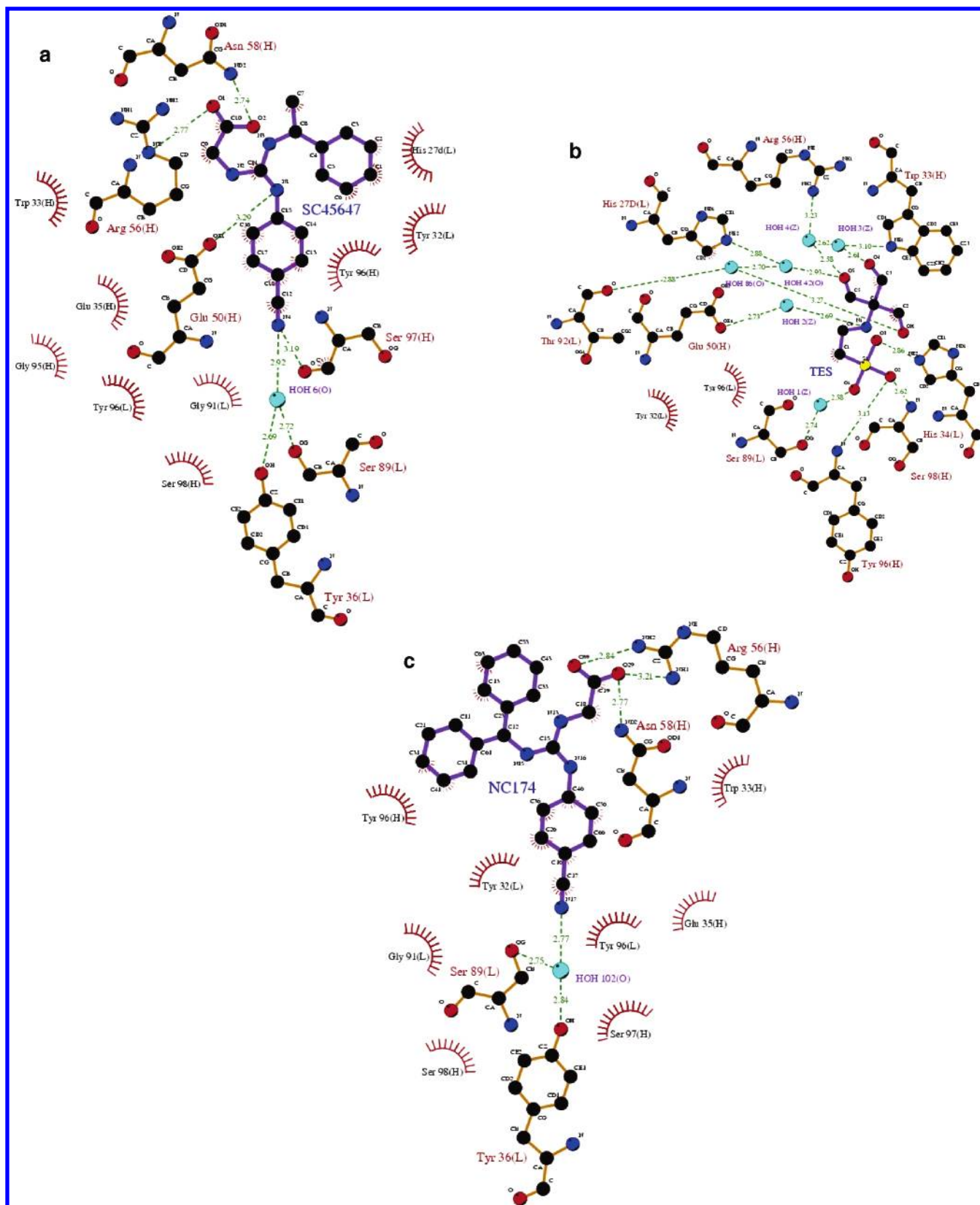


FIGURE 4: (a) Key interactions of high-potency sweetener SC45647 with NC6.8. Interaction patterns for the cyanophenyl and acetyl groups are very similar to NC174, while the hydrophobic group of SC45647 lacks a second phenyl ring at C8 leading to reduced interactions with heavy-chain residues. Note the presence of a chiral center at C8 (*R* conformation). Diagram created using LIGPLOT (47). All LIGPLOT figures are oriented so that the ligands point down into the antigen-binding pocket. (b) Key interactions of nonsweetener TES with NC6.8. Compared to sweet-tasting compounds NC174 and SC45647, the nonsweetener TES exhibits a significantly different binding pattern, dominated by a complex, water mediated hydrogen bond network and only few hydrophobic interactions. (c) Key interactions of super-potency sweetener NC174 with NC6.8. Interaction patterns for the cyanophenyl and acetyl groups are very similar to SC45647 (Figure 4a), while the larger hydrophobic biphenyl group shows stronger hydrophobic interactions with both the L and H chains of NC6.8. For clarity of the plot, a hydrogen bond from N15 to Tyr 96H backbone oxygen has been omitted. Residues from PDB entry 2CGR were renumbered to comply with Kabat nomenclature corresponding to Figure 4a,b.

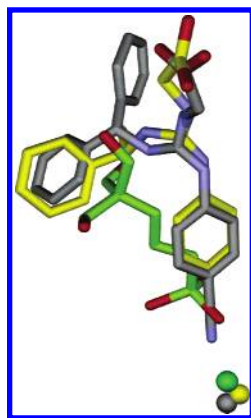


FIGURE 5: Superposition of ligands bound to NC6.8 antibody fragment. Ligands, oriented pointing down into the antigen-binding pocket as in Figures 2 and 4. Gray C atoms: NC174. Yellow C atoms: SC45647. Green C and S atoms: TES. The conserved water atoms participating in the hydrogen bonding to Ser 89L are colored correspondingly. Distinctly visible is the similar positioning of the active groups in the sweeteners, with the exception of the missing second phenyl group in SC45647, which lacks the additional contacts to heavy-chain CDR residues. Superposition based on V domain residues VL1:107 and VH1:113 using LGA (45), figure created with MSI LabViewer Lite and rendered with PovRay 3.5.

and stabilized by hydrogen bonds from the CN group via a conserved water molecule to Ser 98L and Tyr 36L. The possible role of several water molecules in the binding has been discussed for NC174 (22). The deeply buried water atom bridging the CN group to Ser 89L O γ and Tyr 36L O η is clearly visible in all three NC6.8 sweetener complexes. This water atom, however, has not been observed in the NC10.14–NC174 complex (23), and the general role of water mediated contacts in sweetener binding remains open until structures of complexes between tastants and the T1R2 VFTM become available. It is noteworthy though that water mediated contacts do play a significant role in the binding of glutamate to the structurally related metabotropic glutamate receptor (19).

The guanidyl and acetate groups are oriented in similar positions in both binary complex structures (Figure 5). The guanidyl group in NC174 exhibits a strong hydrogen bond to the H chain backbone via Tyr 96H O, an interaction absent in the SC45647 complex. The acetyl groups of both ligands exhibit similar hydrogen bonding patterns, but electron density for the SC45647 acetyl group does show indications for possible secondary conformations consistent with observed minor conformations of the Arg 56H side chain.

Role of the Hydrophobic Group in Glucophore Binding. The structure comparison between Fab complexes suggests a significant role of the hydrophobic group in the interaction of the sweeteners with NC6.8. In 1967, a simple pharmacophore model was proposed (15) stating that every sweetener compound has a hydrogen donor and a hydrogen acceptor group, and the arrangement of the functional hydrogen bond donor and acceptor groups was thought to form antiparallel hydrogen bonds with the receptor. A few years later it was suggested (37) that the presence of a third functional group, a hydrophobic group, is necessary for sweet-tasting molecules. The above hypothesis has been widely accepted, because of its ability to explain the sweetness of many structurally different compounds. In 1996, the multipoint attachment (MPA) theory for human taste

receptors was proposed (38). According to the MPA theory, human taste receptors should contain a minimum of eight binding (recognition) sites occupying the central cavity of the receptor, whose central cavity should be formed by Asp, Lys, Glu, Ser, or Thr residues. Structural data from this study and others (22, 23) confirm that the antigenic epitope is surrounded by multiple charged residues, particularly at the bottom of the receptor binding site, and those residues actively participate in sweetener recognition. Recent studies indicate that most sweeteners likely bind to the T1R2 VFTM region of the heteromeric T1R2/T1R3 taste receptor (14). Exceptions have been established for cyclamate, a low-potency sweetener of the sulfamate class (14), and the taste inhibitor lactisole (18), which bind within the transmembrane region of the taste receptor.

As a result of different size and conformation of the hydrophobic groups of NC174 and SC45647, their specific interactions with residues of the antigenic epitope of NC6.8 vary. In NC174 (Figure 4c) all of the three functional groups (cyanophenyl, triguanidino group, and acetyl group) are positioned favorably to interact with residues of the antigenic epitope of NC6.8. The strong interaction and steric restraints reduce the freedom of rotation around the triguanidino group and restrict movement of the large biphenyl-substituted group of NC174. To accommodate the large biphenyl group of NC174, the antigen-binding pocket of NC6.8 widens compared to the SC45647 complex. In the case of NC174, the phenyl group that corresponds to the single SC45647 phenyl ring interacts with both light-chain and heavy-chain residues, while the single phenyl ring of SC45647 interacts with only light-chain residues (also visible in Figure 3) and is probably less tightly bound as evidenced by slightly higher *B* factors. Differences in conformational freedom and composition of the hydrophobic moieties are thus very likely dominating factors in fine-tuning sweetener potency.

However, the extrapolation of details observed in binding of hydrophobic sweetener moieties in Fab complexes to their actual correspondence in receptor binding needs to be treated with caution. The biphenyl group of NC174 in fact adopts different conformations in the Fab complex with NC6.8 (22) and each of the two copies of NC10.14 (23), which is likely the result of a reduced ability of NC10.14 to lock the biphenyl group in place (23).

Conformational Changes Induced in the Receptor Molecule. Upon binding of NC174, the NC6.8 Fab undergoes an unusually large allosteric conformational change, evidenced by a change in the Fab elbow angle by $\sim 30^\circ$, which has led to reconsideration (22) of the idea of elbow bending as a mechanism for signal transduction from the variable to the constant antibody domains. Although the evidence for such a mechanism in complete antibodies is sparse (39), the NC6.8–NC174 system has been extensively used in molecular dynamics modeling (40).

Interestingly, no significant changes in elbow angle compared to free NC6.8 were calculated for either the high-potency sweetener SC45647 or the nonsweetener TES complex (Table 2). This is also evidenced by a small overall backbone rmsd and visualized in Figure 6. For NC6.8, the large change in elbow angle upon super-sweetener binding seems to be quite unique and may be a result of the particular crystal growth conditions (22). That neither high-potency sweetener SC45647 nor the nonsweetener TES induces a

Table 2: Elbow Angles and Crystallographic Space Group of Antibody Sweetener Complexes^a

crystal structure	PDB code	elbow angle (deg)	space group
NC6.8 (native)	1CGS	189	C2
NC6.8–SC45647	1YNK	188	C2
NC6.8–TES	1YNL	190	C2
NC6.8–NC174	2CGR	152	P ₂ ₁ 2 ₁ 2
NC10.14(LH)–NC174	1ETZ	193	P ₁
NC10.14(AB)–NC174	1ETZ	192	P ₁

^a All Fab elbow angles calculated consistently following the method of Wilson and Stanfield (39) using LGA superpositions (45). Error estimate $\pm 1^\circ$. Angles published for 1ETZ (23) are the complement angles.

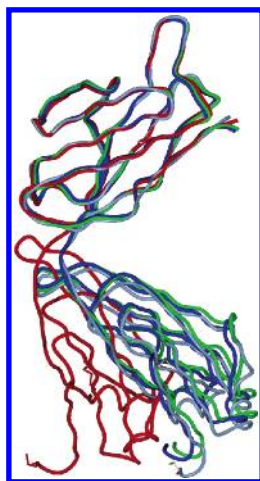


FIGURE 6: Elbow angles of complexed and free NC6.8. Shown are variable domain superpositions of the light chains of free NC6.8 (gray), NC174 (red), SC45647 (blue), and TES (green) complexes. The large change in elbow angle upon formation of the NC174 complex (red) is evident, and no significant changes in elbow angle upon complex formation with SC45647 and TES take place. Superposition on residues 1:107 using LGA (45), figure rendered with ICM Pro (41).

domain orientation change indicates that no simple correlation between sweetener potency and a possible allosteric effect in tastant binding exists for NC6.8. In addition, crystal packing may play a determining role in the elbow angle, as all NC6.8 structures—whether complexed or not—that crystallize in the same space group (C2) have essentially the same elbow angles (Table 2).

Structural studies of the extracellular VFTM domains of mGluR1 (19), homologous to the T1R2 VFTM (23% sequence identity) harboring the major sweetener binding site (14, 16), indicate that ligand binding is in fact accompanied by a substantial intradomain closing of the two lobes of the VFTM domain. Assuming that a similar mechanism is responsible for sweetener binding, it is likely that conformational changes at the VFTM binding site, possibly combined with an interdomain rearrangement of the heterodimeric T1R2/T1R3 receptor, are a key step in the signaling of taste perception.

Upon binding of the sweeteners, local conformational changes in the NC6.8 antigen-binding pocket occur and residues shift to accommodate the ligands. In particular, Tyr 96H significantly moves from the free conformation and covers the binding pocket, while Trp 33H opens the pocket from the free position to accommodate the π -stacking with the guanido groups (Figure 7). Similar patterns of movement

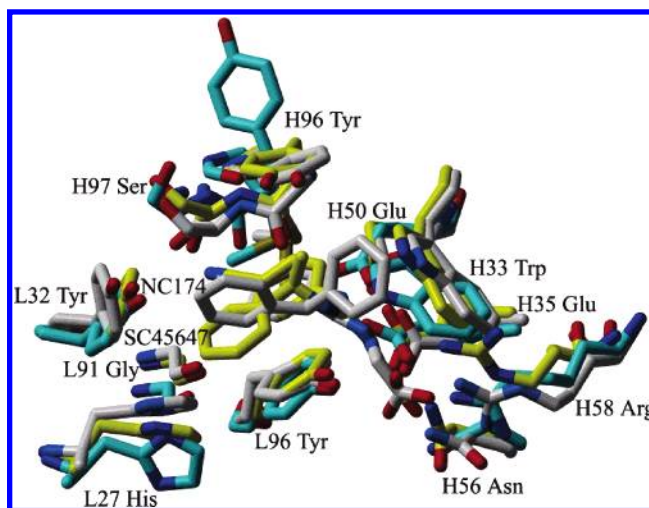


FIGURE 7: Conformational changes of key residues of NC6.8 upon NC174 and SC45647 binding. View down into the antigen-binding pocket. Free NC6.8 C atoms displayed in cyan, complexed conformation and ligand C atoms in gray for NC174 and yellow for SC45647. Distinctly visible is the large conformational change of Tyr 96H covering the ligand-binding pocket, and the reorientation of Trp 33H that π -stacks with the guanidyl group of SC45647 while Tyr 96H π -stacks with the phenyl group of SC45647. The water atoms bridging the CN groups to Ser 89L are buried deep at the bottom of the antigen-binding pocket and are not shown in this figure. Superposition on residues 1:107 using LGA (45), figure rendered with ICM Pro (41).

are also observed for residues His 27L, Arg 58H, and Asn 56H. The remaining antibody residues participating in sweetener binding undergo only smaller displacements from their native conformation.

Nonsweetener (TES) Complexes

In the TES bound structure key residues Trp 33H, His 27L, Arg 56H as well as Glu 50H and Thr 92L interact with TES only indirectly via water molecules, whereas in NC174 and SC45647 complexes these residues interact either directly or via π -stacking and hydrophobic interactions with the respective sweetener compounds. In addition, no hydrophobic group is present in TES. Superposition of the NC6.8–TES complex with the other sweetener complexes reveals that the electronegative sulfonic acid group is located in a similar position as the electronegative cyanophenyl group (Figure 6), located deeply in the antigenic sweetener binding pocket. The water molecule mediating the interaction of the sweetener cyanophenyl groups to Ser 89L is conserved and links the sulfonyl group via O1 to the bottom of the antigen-binding pocket. Compared to the high-affinity sweeteners, the conformational changes induced in NC6.8 upon TES binding are less pronounced than those induced by NC174 and SC45647 sweeteners, and as shown in Figure 4b, most ligand–receptor interactions are indirectly mediated through a complex (and likely more flexible) water network.

Absent in TES is any hydrophobic group, which according to the model of Kier (37) is necessary for sweet-tasting molecules. In order to test whether TES tastes sweet, a blind tasting of distilled water, 100 nM, 1 mM, 10 mM, and 100 mM TES buffer (pH 6.0) was conducted. At no concentration could any sweet taste be established, only a soapy and slightly sour taste perception at 10 and 100 mM, consistent with the proposed requirement of a hydrophobic group for sweet taste perception.

Although TES effectively competes for Fab binding even in the presence of a 100-fold excess of low-potency sweetener compounds including aspartame, it is not able to compete with super- and high-potency sweeteners for NC6.8 binding. TES thus has significantly more affinity toward NC6.8 than low-sweetener compounds, and could act as a sweet taste antagonist or a competitive inhibitor. The question whether TES is a true sweet taste antagonist, implying that it is competitively binding in the same pocket of the taste receptor, or just competing for low-potency sweetener binding in the case of the surrogate Fab model, is difficult to answer from structural data alone. The fact that TES competes successfully also with aspartame, which has been mapped to the N-terminal domain of T1R2 (14) harboring the generic tastant binding site at the VFTM module (16), indicates that TES may in fact act as a sweet taste antagonist for sweeteners binding in the VFTM pocket.

Similarities between the Binding Pockets of the T1R2 Receptor and NC6.8

The amino acid sequences of the mouse T1R2 VFTR domain and mGluR1 were aligned (23% identity), and a basic homology model based on the mGluR1 subunit A (MOL1, closed conformation (19)) was built and refined in ICM Pro (41). The model is of sufficient quality in the core region comprising the conserved binding site. Most geometry violations are located in loops, with overall 85% of residues in the Ramachandran core region, 10% allowed region, and 5% outliers (42). Comparison of the binding pocket of the T1R2 VFTM in the homology model with NC6.8 shows interesting similarities. Both receptor pockets are deep and are formed by two distinct subdomains. In the VFTM structure, the binding site is formed by residues of the two flexibly connected lobes comprising the VFTM, and in NC6.8 residues of both the heavy and the light chain contribute to the binding site (Figure 3). Both binding pockets are covered at the bottom with charged residues, and notably Ser 165(89L), a conserved water molecule, and Tyr 236(96L) form a structurally similar arrangement at the bottom of both binding pockets. In both mGluR1 and NC6.8, the conserved Tyr 236(96L) participates in π -stacking to the ligand. Although the quality of the T1R2 homology model is not sufficient to dock the trisubstituted guanidinium sweeteners with high scores into the T1R2 binding pocket, the pocket shape is remarkably close to the overall shape of the NC174 and SC45647 sweetener molecules (Figure 8), and does allow accommodation of the bulky hydrophobic residues, with aromatic residues available at the opening of the binding pocket that could stabilize the hydrophobic groups of the sweeteners. Probably as a result of the closure of the two lobes of the VFTMs upon ligand binding, additional residues are covering the binding site and prevent the sweetener ligands from exploring the whole pocket space during the docking. Nevertheless, the overall similarities and partial conservation of interactions would indicate that the NC6.8 Fab surrogate is representing most of the crucial features of the T1R2 binding site.

CONCLUSIONS

The availability of antibody–sweetener complexes ranging from super-potency tastants (22, 23) to high-potency and

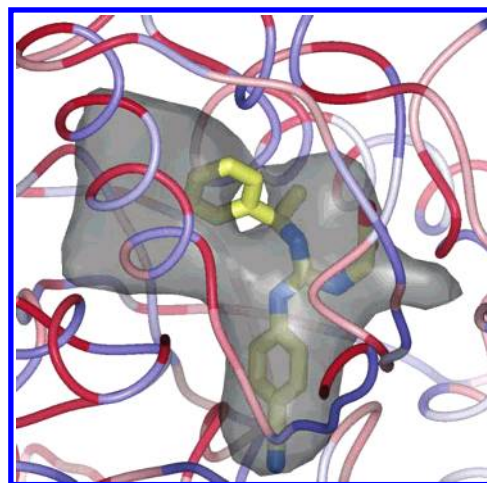


FIGURE 8: Overall shape of binding pocket in T1R2 homology model. The binding pocket (gray transparent shape) of the presumed sweetener binding site located between the two VFTM lobes shows overall shape complementarity to the trisubstituted guanidinium sweeteners and could in principle accommodate the large molecules. Same pocket orientation as NC6.8 Fab binding pocket. Docked in the binding pocket is SC45647 (yellow ball-and-stick model), with the cyanophenyl group occupying the position of the glutamate deep in the binding pocket of the mGluR1 receptor. Homology model, flexible ligand docking and figure created using Molsoft ICM Pro. Ribbon of homology model from mGluR1 colored by conformational energy (blue low, red high) and based on mouse T1R2 sequence (23% aligned identity).

nonsweetening compounds (this study) amplifies the complex nature of receptor interactions involved in sweet taste perception. Sweetener potency is fine-tuned by multiple interactions between specific amino acid residues and the functional groups of the sweeteners. While many details remain to be examined in further structural studies, a consistent picture begins to emerge in identifying key residues and interactions as well as the role of hydrophobic groups in the molecular recognition and for the design of synthetic substituted triguanidine tastants.

Reflecting the chemical complexity of the sweeteners, the receptor–ligand interactions include a complex array of tight hydrogen bonds and charged interactions (Asn 58H, Arg 56H, Glu 50H, Ser 97H, Tyr 96H) and a significant number of hydrophobic contacts, with a substantial contribution of π -stacking (Trp 33H, Tyr 32L). It is very likely that the difference in super- versus high-potency guanidine sweeteners and related zwitterionic low-potency tastants is determined by the nature and conformation of the hydrophobic group. The complex structure with nontastant TES, which effectively competes against low-potency sweeteners (including aspartame that has been mapped to the VFTM region of the T1R2 receptor), shows that although many of the key residues are involved in ligand binding, the interactions are largely mediated via water atoms. In addition, the zwitterionic nontastant TES does not possess any hydrophobic group, emphasizing the necessity of a hydrophobic group in taste perception at the sweetener binding site. Interestingly, a conserved water molecule (bound to Ser 89L and Tyr 36L) buried deeply in the antigen-binding pocket of NC6.8 is involved in the binding of all investigated molecules (super-potency NC174, high-potency SC45647 as well as the nontastant TES), which seems to indicate a role of the conserved water filling the deep bottom of the NC6.8 antigen binding pocket (Figure 3). Indirectly mediated contacts

between ligand and receptor have also been established in the glutamate bound mGluR1 structure (19), a close homologue of the T1R receptor family (20). The conserved water molecule is absent in the NC10.14 complex with NC174 (23), and the exact role of these specific, indirect hydrogen bonded interactions in taste perception remains open at present.

The qualitative correspondence of structural features and interactions between the NC6.8 Fab antigen binding pocket and those in a homology model of the T1R2 VFTM indicate that NC6.8 does present a reasonable surrogate for the T1R2 VFTM binding pocket. Although it is likely that a conformational change in the T1R2 VFTM of the GPCR taste receptor heterodimer is in fact induced upon ligand binding (16, 18), the observed conformational changes (or their absence) in the Fab surrogate models do not necessarily relate directly to substrate-mediated changes in the complex, multidomain taste receptors.

ACKNOWLEDGMENT

We thank the 19-ID beam line support staff at Argonne National Laboratory Structural Biology Center beam lines. Katherine Kantardjieff, CSU Fullerton and W. M. Keck Center for Molecular Structure, has provided assistance with molecular modeling of the T1R2 VFTM. The Advanced Photon source is operated by the U.S. Department of Energy Office Research under Contract No. W-31-109-ENG-88. Lawrence Livermore National Laboratory is operated by the University of California for the U.S. Department of Energy under Contract No. W-7405-ENG-48. This paper is dedicated in memory of Linda Fisher, Texas A&M University, recognizing her invaluable contributions and kind support of students and researchers at the Texas A&M University Biochemistry & Biophysics Department.

REFERENCES

- Inoue, M., McCaughey, S. A., Bachmanov, A. A., and Beauchamp, G. K. (2001) Whole Nerve Chorda Tympani Responses to Sweeteners in C57BL/6ByJ and 129P3/J Mice, *Chem. Senses* 26, 915–923.
- Lindemann, B. (1996) Taste reception, *Physiol. Rev.* 76, 718–766.
- Kinnamon, S. C., and Cummings, T. A. (1992) Chemosensory transduction mechanisms in taste, *Annu. Rev. Physiol.* 54, 715–731.
- Gilbertson, T. A., Damak, S., and Margolskee, R. F. (2000) The molecular physiology of taste transduction, *Curr. Opin. Neurobiol.* 10, 519–527.
- Zhao, G. Q., Zhang, Y., Hoon, M. A., Chandrashekar, J., Erlenbach, I., Ryba, N. J. P., and Zuker, C. S. (2003) The Receptors for Mammalian Sweet and Umami Taste, *Cell* 115, 255–266.
- Pin, J., Galvez, T., and Prezeau, L. (2003) Evolution, structure, and activation mechanism of family 3/C G-protein-coupled receptors, *Pharmacol. Ther.* 98, 325–354.
- Sainz, E., Korley, J. N., Battey, J. F., and Sullivan, S. L. (2001) Identification of a novel member of the T1R family of putative taste receptors, *J. Neurochem.* 77, 896–903.
- Margolskee, R. F. (2002) Molecular mechanisms of bitter and sweet taste transduction, *J. Biol. Chem.* 277, 1–4.
- Chandrashekar, J., Mueller, K. L., Hoon, M. A., Adler, E., Feng, L., Guo, W., Zuker, C. S., and Ryba, N. J. (2000) T2Rs function as bitter taste receptors, *Cell* 100, 703–711.
- Jiang, P., Ji, Q., Liu, Z., Snyder, L. A., Benard, L. M. J., Margolskee, R. F., and Max, M. (2004) The Cysteine-rich Region of T1R3 Determines Responses to Intensely Sweet Proteins, *J. Biol. Chem.* 279, 45068–45075.
- Caldwell, J. E., Abildgaard, F., Dzakula, Z., Ming, D., Hellekant, G., and Markley, J. L. (1998) Solution structure of the thermo-stable sweet-tasting protein brazzein, *Nat. Struct. Biol.* 5, 427–431.
- Spadaccini, R., Crescenzi, O., Tancredi, T., De Casamassimi, N., Saviano, G., Scognamiglio, R., Di Donato, A., and Temussi, P. A. (2001) Solution structure of a sweet protein: NMR study of MNEI, a single chain monellin, *J. Mol. Biol.* 305, 505–514.
- Spadaccini, R., Trabucco, F., Saviano, G., Picone, D., Crescenzi, O., Tancredi, T., and Temussi, P. A. (2003) The mechanism of interaction of sweet proteins with the T1R2-T1R3 receptor: evidence from the solution structure of G16A-MNEI, *J. Mol. Biol.* 328, 683–692.
- Xu, H., Stanszewski, L., Tang, H., Adler, E., Zoller, M., and Li, X. (2004) Different functional roles of T1R subunits in the heteromeric taste receptor, *Proc. Natl. Acad. Sci. U.S.A.* 101, 14258–14263.
- Shallenberger, R. S., and Acree, T. E. (1967) Molecular theory of sweet taste, *Nature* 216, 480–482.
- DuBois, G. E. (2004) Unravelling the biochemistry, *Proc. Natl. Acad. Sci. U.S.A.* 101, 13972–13973.
- Teller, D., Okada, T., Behnke, C., Palczewski, K., and Stenkamp, R. (2001) Advances in determination of a high-resolution three-dimensional structure of rhodopsin, a model of G protein-coupled receptor (GPCRs), *Biochemistry* 40, 7761–7772.
- Jiang, P., Cui, M., Zhao, B., Liu, Z., Snyder, L. A., Benard, L. M., Osman, R., Margolskee, R. F., and Max, M. (2005) Lactisole interacts with the transmembrane domains of human T1R3 to inhibit sweet taste, *J. Mol. Biol.* 280, 15238–15246.
- Kunishima, N., Shimada, Y., Tsuji, Y., Sato, T., Yamamoto, M., Kumasaka, T., Nakanishi, S., Jingami, H., and Morikawa, K. (2000) Structural basis of glutamate recognition by a dimeric metabotropic glutamate receptor, *Nature* 407, 971–977.
- Montmayeur, J. P., Liberles, S., Matsunami, H., and Buck, L. (2001) A candidate taste receptor gene near a sweet taste locus, *Nat. Neurosci.* 4, 492–498.
- Walters, D. E., Orthoefer, F. T., and Dubois, G. E. (1991) in *Sweeteners. Discovery, molecular design and chemoreception* (Walters, D. E., Orthoefer, F. T., and DuBois, G. E., Eds.) pp 214–223, American Chemical Society, Washington, DC.
- Guddat, L. W., Shan, L., Anchin, J. M., Linthicum, D. S., and Edmundson, A. B. (1994) Local and transmitted conformational changes on complexation of an anti-sweetener Fab, *J. Mol. Biol.* 236, 247–274.
- Guddat, L. W., Shan, L., Broomell, C., Ramsland, P. A., Fan, Z.-C., Anchin, J. M., Linthicum, D. S., and Edmundson, A. B. (2000) The three-dimensional structure of a complex of a murine Fab (NC10.14) with a potent sweetener (NC174): an illustration of structural diversity in antigen recognition by immunoglobulins, *J. Mol. Biol.* 302, 853–872.
- Anchin, J. M., Nagarajan, S., Carter, J., Kellog, M. S., DuBois, G. E., and Linthicum, D. S. (1997) Recognition of Superpotent Sweetener Ligands by a Library of Monoclonal Antibodies, *J. Mol. Recognit.* 10, 235–242.
- Nofre, C., Tinti, J. M., and Ouar-Chatzopoulos, E. (1990), Université Claude Bernard, Lyon 1, France, US Patent 4,921,939.
- Liu, H., Smith, T. J., Lee, W. M., Mosser, A. G., Rueckert, R. R., Olson, N. H., Cheng, R. H., and Baker, T. S. (1994) Structure determination of an Fab fragment that neutralizes human rhinovirus 14 and analysis of the Fab-virus complex, *J. Mol. Biol.* 240, 127–137.
- Parham, P., Androlewicz, M. J., Brodsky, F. M., Holmes, N. J., and Ways, J. P. (1982) Monoclonal antibodies: purification, fragmentation and application to structural and functional studies of class I MHC antigens, *J. Immunol. Methods* 53, 133–173.
- McPherson, A. (1982) *Preparation and analysis of protein crystals*, Krieger Publishing Company, Malabar, FL.
- Otwinowski, Z., and Minor, W. (1997) Processing of X-ray Diffraction Data Collected in Oscillation Mode, *Methods Enzymol.* 267, 307–326.
- Matthews, B. W. (1968) Solvent content of protein crystals, *J. Mol. Biol.* 33, 491–497.
- Kantardjieff, K. A., and Rupp, B. (2003) Matthews coefficient probabilities: Improved estimates for unit cell contents of proteins, DNA, and protein-nucleic acid complex crystals, *Protein Sci.* 12, 1865–1871.
- Brünger, A. T., Adams, P. D., Clore, G. M., DeLano, W. L., Gros, P., Grosse-Kunstleve, R. W., Jiang, J. S., Kuszewski, J., Nilges,

- M., Pannu, N. S., Read, R. J., Rice, L. M., Simonson, T., and Warren, G. L. (1998) Crystallography & NMR System: A New Software Suite for Macromolecular Structure Determination, *Acta Crystallogr. D54*, 905–921.
33. McRee, D. E. (1999) XtalView/Xfit—A versatile program for manipulating atomic coordinates and electron density, *J. Struct. Biol.* 125, 156–165.
34. Reddy, V., Swanson, S., Sacchettini, J. C., Kantardjieff, K. A., Segelke, B., and Rupp, B. (2003) Effective electron density map improvement and structure validation on a Linux multi-CPU web cluster: The TB Structural Genomics Consortium Bias Removal Web Service, *Acta Crystallogr. D59*, 2200–2210.
35. Murshudov, G. N., Vagin, A. A., and Dodson, E. D. (1997) Refinement of Macromolecular Structures by the Maximum-Likelihood Method, *Acta Crystallogr. D53*, 240–255.
36. Kabat, E. A., Wu, T. T., Perry, H. M., Gottesman, K. S., and Foeller, C. (1992) *Sequences of Proteins of Immunological Interest*, 5th ed., Public Health Services, NIH, Washington, DC.
37. Kier, L. B. (1972) A molecular theory of sweet taste, *J. Pharm. Sci.* 61, 1394–1397.
38. Nofre, C., Tinti, J. M., and Glaser, D. (1996) Evolution of the sweetness receptor in primates. II. Gustatory responses of non-human primates to nine compounds known to be sweet in man, *Chem. Senses* 21, 747–762.
39. Wilson, I. A., and Stanfield, R. L. (1994) Antibody-antigen interactions: new structures and new conformational changes, *Curr. Opin. Struct. Biol.* 4, 857–867.
40. Sotriffer, C. A., Rode, B. M., Varga, J. M., and Liedl, K. R. (2000) Elbow Flexibility and Ligand-Induced Domain Rearrangements in Antibody Fab NC6.8: Large Effects of a Small Hapten, *Biophys. J.* 79, 614–628.
41. Abagyan, R., Totrov, M., and Kuznetsov, D. (1994) ICM: a new method for protein modeling and design. Applications to docking and structure prediction from the distorted native conformation, *J. Comput. Chem.* 15, 488–506.
42. Laskowski, R. A., MacArthur, M. W., Moss, D. S., and Thornton, J. M. (1993) PROCHECK: a program to check the stereochemical quality of protein structures, *J. Appl. Crystallogr.* 26, 283–291.
43. Engh, R. A., and Huber, R. (1991) Accurate bond and angle parameters for X-ray structure refinement, *Acta Crystallogr. A47*, 392–400.
44. Cruickshank, D. W. J. (1999) Remarks about protein structure precision, *Acta Crystallogr. D55*, 583–601.
45. Zemla, A. (2003) LGA: a method for finding 3D similarities in protein structures, *Nucleic Acids Res.* 31, 3370–3374.
46. Merritt, E. A., and Bacon, D. J. (1997) Raster3D: Photorealistic molecular graphics, *Methods Enzymol.* 277, 505–524.
47. Wallace, A. C., Laskowski, R. A., and Thornton, J. M. (1995) LIGPLOT: a program to generate schematic diagrams of protein–ligand interactions, *Protein Eng.* 8, 127–134.

BI050613U